Jacob C. Badger
Department of Mechanical Engineering,
Brigham Young University,
Provo, UT 84602
e-mail: j_badger@byu.edu

Todd G. Nelson
Department of Engineering,
University of Southern Indiana,
Evansville, IN 47712
e-mail: tgnelson@usi.edu

Robert J. Lang
Lang Origami,
Alamo, CA 94507
e-mail: robert@langorigami.com

Denise M. Halverson
Department of Mathematics,
Brigham Young University,
Provo, UT 84602
e-mail: halverson@math.byu.edu

Larry L. Howell[1]
Department of Mechanical Engineering,
Brigham Young University,
Provo, UT 84602
e-mail: lhowell@byu.edu

Normalized Coordinate Equations and an Energy Method for Predicting Natural Curved-Fold Configurations

Of the many valid configurations that a curved fold may assume, it is of particular interest to identify natural—or lowest energy—configurations that physical models will preferentially assume. We present normalized coordinate equations—equations that relate fold surface properties to their edge of regression—to simplify curved-fold relationships. An energy method based on these normalized coordinate equations is developed to identify natural configurations of general curved folds. While it has been noted that natural configurations have nearly planar creases for curved folds, we show that nonplanar behavior near the crease ends substantially reduces the energy of a fold. [DOI: 10.1115/1.4043285]

Keywords: curved folding, origami, developable, energy

1 Introduction

In recent years, the ancient art of origami has been revolutionized by modern technology. Many methods have been developed to design, adapt, and analyze origami patterns for both artistic and engineering applications [1–6]. Several applications have made use of interesting energy characteristics exhibited by origami and kirigami patterns [7–10]. While *polyhedral folding*—folding where all creases are straight and surfaces are planar—has become fairly well-defined, *curved folding*—folding where creases are curved and surfaces are allowed to bend—remains relatively enigmatic. A great deal of the mystery surrounding curved folding is due to the infinite number of unique configurations a curved fold can assume. While many remarkable methods have been developed to model specific configurations of curved folds under certain constraints [11–13], it remains challenging to predict the natural configurations that physical models will assume.

To this end, we begin with a review of the fundamentals of curved folding and introduce the notation we use throughout this paper. We then simplify curved-fold calculations by utilizing normalized coordinate equations—equations that relate properties of a curved fold at a point to the normalized distance from the point to the edge of regression. From these normalized coordinate equations, we develop an energy method that can be used to find natural configurations for a general curved fold.

Using this energy method, we make two surprising observations. First, it was conjectured by Fuchs and Tabachnikov [14] that general curved folds naturally assume planar, constant fold angle configurations. We observe that natural configurations of various simple folds, while close, are not planar or uniform. This observation is verified with the help of physical models. Second, we observe that although the natural configurations of a quarter-circular fold are neither planar nor uniform, remarkably, the rulings appear to remain geodesically fixed as the stiffness of the material and the initial fold angle are varied.

2 Background

As shown by Duncan and Duncan [15], curved folds form naturally when a thin sheet of material is yielded along a curved line called a crease. As the crease is plastically deformed to a nonzero fold angle (γ), the material on either side bends without ripping, tearing, or stretching to take a 3D folded form as shown in Fig. 1. Because ripping, tearing, and stretching are high-energy cost activities compared to bending, the material on either side of a folded crease preferentially takes the form of curved developable surfaces. A developable surface is a singly curved surface which can be unfolded to a plane through bending only [16]. Thus, a curved

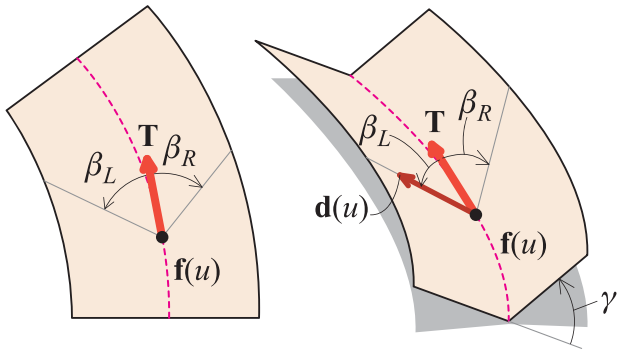

Fig. 1 Illustration of a curved fold formed by folding along a curve f(u) in an unfolded configuration (left) and folded with a fold angle γ (right)

[1]Corresponding author.

Contributed by the Applied Mechanics Division of ASME for publication in the Journal of Applied Mechanics. Manuscript received January 17, 2019; final manuscript received March 21, 2019; published online April 12, 2019. Assoc. Editor: Yihui Zhang.

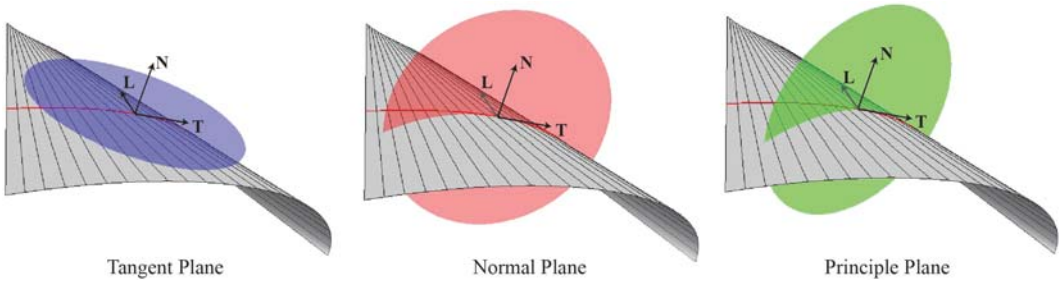

Fig. 2 Tangent (left), normal (center), and principle (right) planes to a curve embedded in a developable surface. These planes contain the geodesic curvature (κ_g), the normal curvature (κ_n), and the principle curvature (κ_p), respectively.

fold consists of two developable surfaces joined by a curved crease in such a way that the entire fold is globally developable or can be unfolded to a flat plane.

Several measures of the crease are useful in describing the relationship between the crease and the curved panels. These include torsion (τ) along with several measures of curvature including the geodesic curvature (κ_g), the normal curvature (κ_n), and the principle curvature (κ_p). As these quantities are well-defined in the field of differential geometry, we will forgo rigorous definitions of these terms and focus on their geometric significance with respect to curved folding. The geodesic curvature (of the crease), κ_g, is a measure of the curvature of the crease contained within the fold surfaces, or the portion of the curvature vector contained in a tangent plane (see Fig. 2, left). Thus, the geodesic curvature can be understood as the curvature of the crease when the curved fold is unfolded to a plane. As long as a crease remains geodesically fixed in the material, the geodesic curvature is a property of the 2D crease pattern and thus invariant for any fold state a curved fold may assume. The normal curvature, κ_n, measures the portion of the curvature of the crease contained in the normal plane to the fold surfaces (see Fig. 2, center). This quantity can be visualized as the portion of curvature that is added to the crease as a result of folding (thus, $\kappa_n = 0$ when the crease is fully unfolded). Whereas the geodesic curvature and the normal curvature were properties of a curve embedded in a surface (in our case, the crease); the principle curvature (κ_p) measures the amount the surface curves in the direction of the greatest curvature. It is important to note that since the crease will generally not follow the direction of the greatest curvature (although such creases, called cross-curves, have particularly nice properties as noted by Lang et al. [17]), the principle curvature along the crease is not a measure of the curvature in the crease.

A great deal of work has been done to analyze, approximate, and model the developable surfaces that result from curved folding. While many valid representations exist including Ref. [18], one common form is the directrix-director (generator) parameterization [19]

$$\mathbf{S}(u, v) = \mathbf{f}(u) + v\mathbf{d}(u) \tag{1}$$

where u and v are the parameters of the surface. When u is held constant, the general form becomes the equation of a line parameterized by v. These lines are called *rulings* or generators. The directrix of the surface is $\mathbf{f}$, and the directors are given by $\mathbf{d}$ (see Fig. 1).

As developable surfaces consist of ruling lines joined together, they form a subset of ruled surfaces. While Eq. (1) describes a general ruled surface, specializing the directrix and directors can represent four fundamental types of developable surfaces. Three of the fundamental types are curved and include generalized cylinders where the rulings are parallel to each other, generalized cones where the rulings meet at a single point, and tangent developables where the rulings are tangent to a space curve called the *edge of regression*. While the edge of regression is commonly used to refer to the curve to which all rulings are tangent, this concept can be generalized to include the apex of a generalized cone and a curve at infinity for a generalized cylinder. Thus, when we refer to the edge of regression, we do not restrict ourselves to tangent developable surfaces but include the singular points of all three classes of curved developable surfaces. The fourth fundamental type is the plane, where rulings can take arbitrary orientations and positions.

Methods have been developed to relate specific valid crease–surface pairs such as the principal of reflection [20], optical-ray parallels [21], and a distance-sum condition [17]. More general numerical approaches have been explored to expand the range of valid crease–surface pairs which can be used in designing curved folds [11,12].

Within the space of curved folding, it becomes of interest to know the minimum energy state a fold will take. The corresponding analysis necessarily considers the curved crease, surfaces on each side, and their boundaries. One energy minimization approach is found in the doctoral work of Dias [22] in modeling the Bauhaus concentric fold pattern. While it has been noted that even paper curved folds exhibit tendencies to move to this minimum energy state, this behavior becomes more pronounced when materials with higher bending stiffness are used [23].

3 Methods

Two of the most notable differences between curved and straight fold origami are (1) the fold angle (γ) of curved folds can vary along the crease and (2) the crease is allowed to bend out of the plane as it is folded as measured by the torsion (τ). Furthermore, these two curved-fold properties—fold angle (γ) and torsion (τ)—are independent of one another, allowing a single curved fold to assume infinitely many unique configurations. Defining a specific configuration of a given curved crease, therefore, requires that both fold angle and torsion functions be defined along the length of the crease.

Although the fold angle and torsion functions are sufficient to define the shape of a folded configuration, in most practical applications, curved folds have finite edges that are fixed within the paper. Thus, the domain of parameterization must be restricted to some finite region. As a curved fold transitions through its diverse configurations, its ruling field often shifts, changing the region of the domain on which the parameterization is defined. Accounting for the variability in the restricted domain can prove challenging. In many applications, this added complexity has been largely avoided by focusing on curved creases where all creases and ruling lines remain fixed within the paper—but, as the field of curved folding advances, the need for a more general approach becomes increasingly apparent.

For the remainder of this paper, we simplify curved fold relationships through the use of normalized coordinate equations. We then present a method for restricting the domain for an arbitrary fold configuration so that the boundary of the restricted domain corresponds to the edge of the fold. Equipped with these tools, we present an

energy method that can be used to predict natural configurations of curved folds.

3.1 Normalized Coordinate Equations. Developable surfaces are typically defined in the directrix-director form given by Eq. (1), with the edge of regression as the directrix. Because all rulings are tangent to the edge of regression (excluding the degenerate cases of cone and cylinder developable surfaces), this single curve encapsulates all information about the developable surface and greatly simplifies surface properties and calculations. However, when defining curved fold surfaces, the curved crease is typically chosen as the directrix because it allows a single directrix to be used for both left and right surfaces. This representation thus simplifies the relationship between fold surfaces. The following normalized coordinate equations are based on a crease-directrix parameterization but incorporate information about the edge of regression to simplify crease relationships.

We can define both sides of our curved fold using the standard crease parameterization as

$$\begin{aligned}\mathbf{S}_L(u, v) &= \mathbf{f}(u) + v\mathbf{d}_L(u)\\ \mathbf{S}_R(u, v) &= \mathbf{f}(u) + v\mathbf{d}_R(u)\end{aligned} \tag{2}$$

where $\mathbf{f}$ is the curved crease and $\mathbf{d}$ gives the ruling directions. For generality, we allow $\mathbf{f}$ to be an arbitrary speed curve and denote the curve speed $\dot{s}$ such that $\dot{s} = \|\mathbf{f}'\|$. For simplicity, we assume that $\mathbf{d}(u)$ has unit length.

For a given configuration of a curved fold, the ruling directions $\mathbf{d}(u)$ are determined by the ruling angle $\beta(u)$—the angle between $\mathbf{d}(u)$ and the tangent of $\mathbf{f}$ at u. To avoid distinguishing between left and right fold surfaces and to simplify notation, we use the convention that the left ruling angle will always be positive and the right ruling angle negative. Thus, the ruling angle β can be calculated using the equations modified slightly from Ref. [14]

$$\begin{aligned}\beta_L &= \left[\cot^{-1}\left(\frac{\tau + \gamma'/(2\dot{s})}{\kappa \csc(\gamma/2)}\right) \bmod \pi\right]\\ \beta_R &= -\left[\cot^{-1}\left(\frac{\tau - \gamma'/(2\dot{s})}{\kappa \csc(\gamma/2)}\right) \bmod \pi\right]\end{aligned} \tag{3}$$

This implies that $\beta_L \in (0, \pi)$ and $\beta_R \in (-\pi, 0)$. Thus, all equations will be given in terms of a general β but are applicable to both fold surfaces.

To measure properties of the fold surfaces such as embedded curve length, area, and mean and Gaussian curvatures, it is convenient to calculate the first and second fundamental surface forms. For a rigorous definition, derivation, and explanation of these forms, the reader is referred to Ref. [24]. In our setting, the coefficients of the first fundamental form (modified from [22]) can be expressed as

$$\begin{aligned}E(u, v) &= \dot{s}^2 + v\left(\dot{s}\kappa_g(u) + \beta'(u)\right)\\ &\quad \cdot \left[v\left(\dot{s}\kappa_g(u) + \beta'(u)\right) - 2\dot{s}\sin\beta(u)\right]\\ F(u, v) &= \dot{s}\cos\beta(u)\\ G(u, v) &= 1\end{aligned} \tag{4}$$

and the coefficients of the second fundamental form as

$$\begin{aligned}|e(u, v)| &= \dot{s}^2\kappa_n(u) - v\dot{s}\left(\dot{s}\kappa_g(u) + \beta'(u)\right)\\ &\quad \cdot \left[\kappa_n(u)\sin\beta(u) - \left(\tau(u) + \frac{\gamma'(u)}{2\dot{s}}\right)\cos\beta(u)\right]\\ f(u, v) &= g(u, v) = 0\end{aligned} \tag{5}$$

where κ_g is the geodesic curvature and κ_n is the normal curvature. These equations offer a concise foundation upon which we can build an intuitive description of a developable surface. To begin to develop this intuition, we relate these equations to the edge of regression.

To locate the edge of regression, we can take advantage of the fact that the principal curvature is undefined along its entire length. It can be shown through Eqs. (4) and (5) that the magnitude of the principle curvature κ_p is given by

$$|\kappa_p(u, v)| = \frac{\kappa_n(u)\csc\beta(u)}{\sin\beta(u) - v\left(\kappa_g(u) + \beta'(u)/\dot{s}\right)} \tag{6}$$

The singularities of this function will therefore lie on the edge of regression. Thus, we can recover the edge of regression by finding the values of u and v for which the denominator is zero. Solving for such points v in terms of u gives the distance from the crease to the edge of regression at each point u—we denote this distance as v_0. The resulting equation for v_0 can then be written as

$$v_0(u) = \frac{\sin\beta(u)}{\kappa_g(u) + \beta'(u)/\dot{s}} \tag{7}$$

The edge of the regression curve ξ can then be found by substituting v_0 into Eq. (1), yielding

$$\xi(u) = \mathbf{f}(u) + \frac{\sin\beta(u)}{\kappa_g(u) + \beta'(u)/\dot{s}}\mathbf{d}(u) \tag{8}$$

This equation alone tells us little about the developable surface of interest, but by substituting (7) into the first fundamental form (4), we obtain a simplified form

$$\begin{aligned}E(u, v) &= \dot{s}^2\left[\cos^2\beta(u) + \left(\frac{v_0(u) - v}{v_0(u)}\right)^2\sin^2\beta(u)\right]\\ F(u, v) &= \dot{s}\cos\beta(u)\\ G(u, v) &= 1\end{aligned} \tag{9}$$

To illustrate the simplicity this formulation can enable, we consider the Riemann area metric (or Jacobian)

$$\sqrt{EG - F^2} = \dot{s}\left(\frac{v_0(u) - v}{v_0(u)}\right)|\sin\beta(u)| \tag{10}$$

The second factor on the right-hand side is of particular interest—it is the ratio of the distance along a ruling line from a point to the edge of regression over the distance along the same ruling line from the crease to the edge of regression (see Fig. 3). In other words, it is the normalized distance that the point lies from the edge of regression.

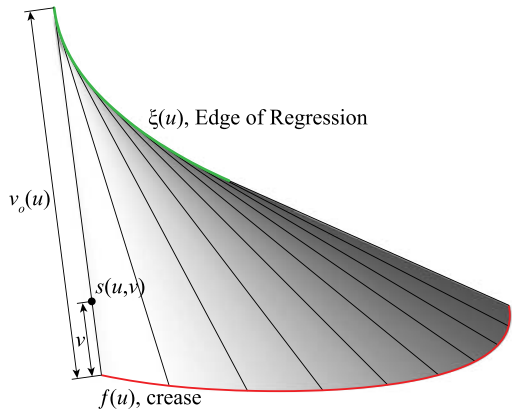

Fig. 3 Normalized distance of a point from the edge of regression

We will denote this normalized distance as

$$\Upsilon(u, v) = \frac{v_0(u) - v}{v_0(u)} \tag{11}$$

Thus, the area metric at a point (u, v) is the curve speed multiplied by the sine of the ruling angle (a measure of the perpendicularity of the ruling lines to the crease) scaled by its normalized coordinate Υ.

Similarly, we can express the principle curvature in terms of Υ as

$$\kappa_p(u, v) = \frac{\kappa_n(u) \csc^2 \beta(u)}{\Upsilon(u, v)} \tag{12}$$

but, as Lang et al. noted [17], the principle curvature along the crease is

$$\kappa_p(u) = \kappa_n(u) \csc^2 \beta(u) \tag{13}$$

Therefore, Eq. (12) takes the form

$$\kappa_p(u, v) = \frac{\kappa_p(u)}{\Upsilon(u, v)} \tag{14}$$

revealing that the principle curvature at any point is independent of the curve speed and is given by the principle curvature along the crease, scaled by the reciprocal of its normalized coordinate Υ. As we will soon see, this relationship will greatly simplify the energy analysis.

While we do not derive any additional normalized coordinate relationships in this paper, we note that many complex equations—including the geodesic equation—can be reduced through the use of normalized coordinates.

3.2 Energy Analysis. A great deal of the difficulty associated with solving for minimal energy configurations lies in restricting the domain of parameterization of fold surfaces under constantly shifting domains of parameterization. Here, we develop a method for restricting the domain of fold surfaces for a general configuration.

In calculating the energy of a curved fold, we consider two types of energy: *bending energy* and *crease energy*. However, since our analysis thus far has considered a curved fold as the union of infinitesimally thin developable surfaces without specified material properties, we will focus on primarily on nondimensional forms of the bending and crease energies. As shown in Ref. [22], formulations of bending and crease energies with appropriate energy units may be obtained by multiplying the nondimensional forms by the bending modulus and stiffness, respectively. The energy method presented here uses the nondimensional energy forms but introduces a stiffness coefficient K to properly scale the contribution of bending and crease energies. This energy method can be used to find the natural configuration of a general curved fold.

3.2.1 Restricting the Fold Domain. To compare the energy of a single curved crease in various folded states where the ruling lines are free to shift, we need to be able to restrict the domain such that fold edges remain fixed within the paper.

To find the boundary of the restricted domain, R, we begin by parameterizing the unfolded edge in terms of the crease and its normal vectors. If we denote the unfolded edge χ, we can write

$$\chi(u) = \mathbf{f}(u) + \ell(u)\mathbf{N}(u) \tag{15}$$

where $\mathbf{N}$ is the unit normal vector to the crease and $\ell(u)$ is the distance along the normal that the edge lies from the crease at each point u. We could, at this point, solve for points along the edge of the folded form by calculating geodesics in the left normal directions, but solving the nonlinear differential equation that defines geodesics is difficult and computationally expensive. Fortunately, we can reduce this to a nonlinear root finding problem by reconstructing the flat ruling field and solving for the edge in the unfolded form.

To formulate this flat edge approach, we consider a single point on the unfolded edge, $\chi(u_0)$, as shown in Fig. 4. Our approach defines a function $D(u)$ that gives the distance along the crease normal at u_0 at which a ruling line, originating at a point on the crease $f(u)$, intersects that normal. From basic trigonometric relationships and the law of sines, it can be shown that

$$D(u) = \frac{(x_0 - x(u)) \sin\big(\theta(u) + \beta(u)\big) - \big(y_0 - y(u)\big) \cos\big(\theta(u) + \beta(u)\big)}{\cos\big(\theta(u) + \beta(u) - \theta_0\big)} \tag{16}$$

where θ is the turning angle of the crease (see Ref. [24]). To calculate the u coordinate of the edge point $\chi(u_0)$, we therefore find the root of the equation

$$D(u) = \text{sign}(\beta)\ell_0 \tag{17}$$

By again applying the law of sines, we show that the v coordinate of the edge point is given as follows:

$$v = \frac{(x_0 - x(u)) \cos\theta(u) + \big(y_0 - y(u)\big) \sin\theta(u)}{\cos\big(\theta(u) + \beta(u) - \theta_0\big)} \tag{18}$$

Edge curves are then approximated by solving for the parameters u and v for a sufficient number of edge points and interpolating the resulting set of v coordinates in terms of u. The resulting edge functions provide the boundary of the restricted domain R, on which we can perform energy calculations.

3.2.2 Bending Energy Calculations. We define the bending energy of a surface as the energy required to bend the surface from a plane. It has been shown [12,25] that the nondimensional bending energy E_B can be calculated using the formula

$$E_B = \int_{\mathbf{R}} \kappa_p^2 \, d\mathbf{A}$$

For a curved fold surface parameterized in the form of Eq. (2), this integral becomes (by substituting Eq. (14) and evaluating the Jacobian)

$$E_B = \iint \frac{\kappa_p^2(u)}{\Upsilon(u, v)} |\sin\beta(u)| \, \dot{s} \, dv \, du \tag{19}$$

The bounds of integration here are the edge functions found in Sec. 3.2.1. These bounds vary depending on the shape of the fold surfaces and orientation of the ruling field, but in general, the integral is straightforwardly calculated by dividing it into sections. Note that when $\Upsilon(u, v) = 0$, the bending energy function has a singularity. This is because $\Upsilon(u, v) = 0$ corresponds to the edge of regression

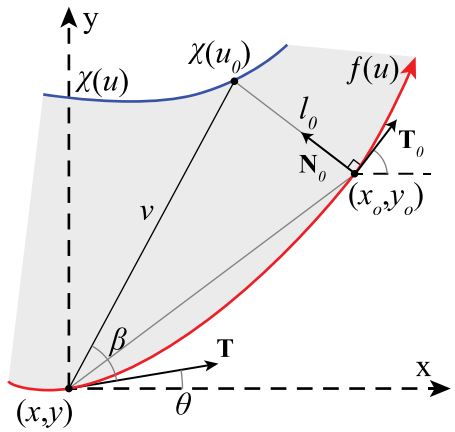

Fig. 4 Solution process for obtaining u, v parameterization of an edge point $\chi(u_0)$

which is known to be singular. Thus, we will consider only fold configurations for which $\Upsilon(u, v) > 0$ on the entire fold domain.

3.2.3 Crease Energy Calculations. Crease energy is the energy needed to change the fold angle from a yielded stable angle which we call the initial fold angle. Various formulations of crease energy exist including those found in Refs. [22,26]. We adopt the formulation in Ref. [22], giving the nondimensional crease energy as

$$E_C = \frac{K}{2}\int_{u_i}^{u_f}\left(\cos\frac{\gamma(u)}{2} - \cos\frac{\gamma_0}{2}\right)^2 du \tag{20}$$

where K is a nondimensional stiffness factor defined as the ratio of material stiffness to the bending modulus and γ_0 is the preset angle. For the purposes of this paper, we assume that the values K and γ_0 are constant along a fold. These values are dependent on material and manufacturing, and the method could be extended to allow them to vary along a curved fold. In Sec. 4.2, we use a variety of parameter values to calculate crease energy and observe a surprising phenomena—in the case of a circular crease, the values of the stiffness factor (K) and preset angle (γ_0) have little to no effect on the ruling field of the optimized crease.

3.3 Optimization. To solve for a minimal energy state, we use a calculus of variations approach, using a set of basis functions to define the torsion and fold angle along a curved fold. The coefficients of these basis functions are varied to minimize the sum of the bending and crease energies.

We use a degree-6 Legendre polynomial basis with distinct sets of coefficients to represent fold angle and torsion functions, giving a total of 14 free variables (including coefficients for the zeroth degree basis functions). We define the objective function for this optimization problem to be the sum of the left and right bending energies (in the form of Eq. (19)) and the crease energy (in the form of Eq. (20)). The objective function for a specific curved crease is then given by

$$E_{\text{total}} = E_{B,L}(\gamma, \tau) + E_{B,R}(\gamma, \tau) + E_C(\gamma) \tag{21}$$

where $E_{B,L}$ and $E_{B,R}$ are the bending energies of the left and right surfaces, respectively. In addition, we define the nonlinear constraint

$$\min_{(u,v)\in\partial R} \Upsilon(u, v) > 0 \tag{22}$$

to ensure that the energy function is defined at every step. This constraint, mentioned in Sec. 3.2.2, can be interpreted physically as ensuring that the edge of regression does not lie in the restricted fold domain—implying the resulting fold surfaces are nonsingular.

4 Results

The energy method described above is applied to identify natural configurations of various curved folds. In Sec. 4.1, we show that the lowest energy state of this specific curved crease, while close to planar, is not necessarily a planar uniform fold as conjectured by Fuchs and Tabachnikov [14]. Similar nonplanar results have recently been observed in Refs. [13,27,28] using elastica-surface generation and finite element methods. Given that the lowest energy state of a circular crease is not planar, we find a natural configuration for the crease. Results for various noncircular and variable width creases are then compared to physical models. Finally, we contextualize our observations of nonplanar behavior by analyzing how the location of the edge of regression affects fold energy.

4.1 Nonplanar, Uniform Folds. Various authors [14,17,22] have observed that folds tend toward configurations with zero torsion (planar) and a constant fold angle (uniform). This planar-uniform behavior appears to hold when the width of the fold surfaces is small compared to the total length of the crease but is clearly contradicted when the width of the fold surfaces is comparable to the crease length. To observe this behavior, try folding along a circle or parabola where the edge extends nearly to the focus. It then becomes apparent that this planar, constant fold angle assumption no longer applies. To verify this observation, we consider two distinct fold surface widths for the quarter-circle crease, shown in Figs. 5 and 7.

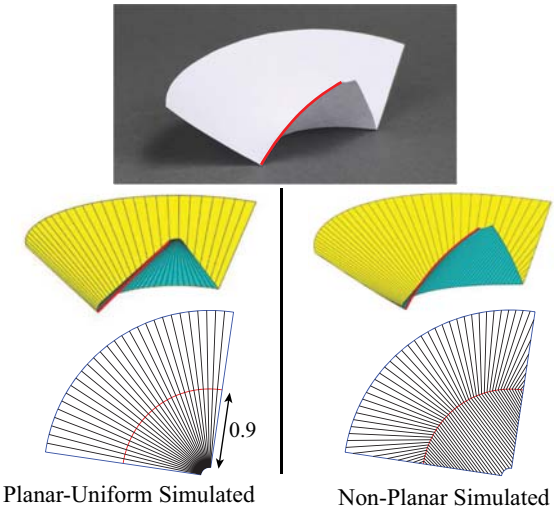

Fig. 5 Physical model of a circular crease of width 0.9 units (top) with the simulated planar-uniform fold and ruling field (left) and simulated minimal-energy uniform fold and ruling field (right). Both simulated configurations have fixed fold-angle $\gamma = \pi/2$.

We begin by considering fold surfaces of width 0.9 on either side of the crease and assume that the fold remains uniform, fixing the fold angle at $\gamma = \pi/2$. While assuming the fold angle to be fixed requires that crease energy be neglected, our intention is to first investigate the common observation that folds tend toward a planar configuration for a constant fold angle by examining the capability of varying torsion in a crease to reduce the total energy independent of the fold angle.

Applying the optimization routine with an initial guess of zero torsion reveals that the lowest energy state is not planar. In fact, by adding torsion to the ends of the curved crease, we are able to reduce the bending energy in the surface by 64%. The optimized result is compared to both a planar-uniform fold and a physical model in Fig. 5. As shown in the figure, the optimized fold shows a high degree of fidelity to the physical model—which can most

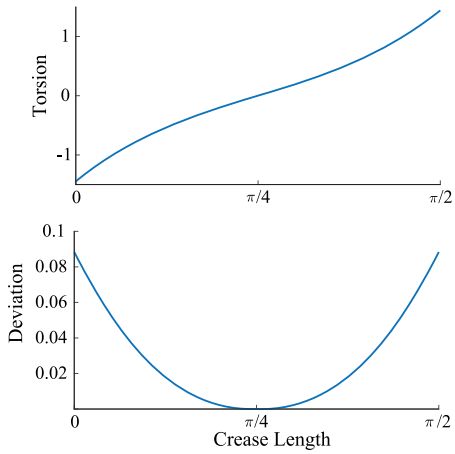

Fig. 6 Optimized torsion function (top) and planar deviation (bottom) for a thin circular crease of width 0.9 units with a fixed fold-angle $\gamma = \pi/2$

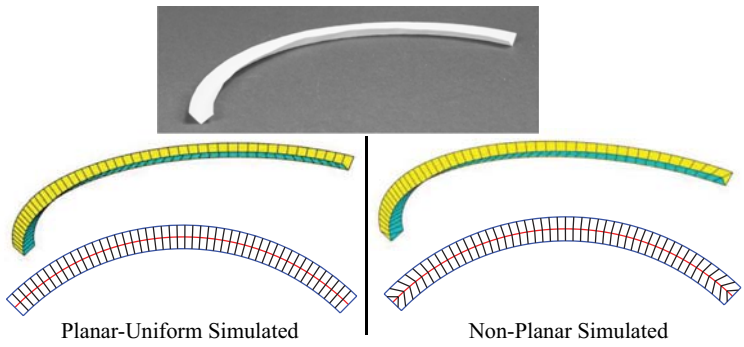

Fig. 7 Physical model of a circular crease of width 0.05 units (top) with the simulated planar-uniform fold and ruling field (left) and simulated minimal-energy uniform fold and ruling field (right). Both planar-uniform and minimal-energy uniform folds have fixed fold-angle $\gamma = \pi/2$.

easily be seen by comparing the inner edges of the folds (marked for clarity). The torsion and resulting planar deviation depicted in Fig. 6 for the optimized fold clearly illustrate that the resulting configuration is nonplanar. The reason for the significant decrease in energy will be further analyzed in Sec. 4.4.

We now turn our attention to the case when the width of the fold surfaces is small, by reducing the width of fold surfaces to 0.05 units. This time, bending energy is reduced by about 4%. The optimized result is compared to both a planar-uniform fold and a physical model in Fig. 7.

We note here that the greatest effect of the optimized torsion on the shape of the fold is not in deforming the crease out of the plane but rather in shifting the ruling field and therefore the location of the edge of regression. For this reason, it can be difficult to visually distinguish the optimized crease from a planar crease. This phenomena is observed in Fig. 8, where the optimized torsion function is compared to the magnitude of the distance that the folded crease deviates from a plane. From Figs. 7 and 8, we observe that while the crease deviates only slightly from a plane, the ruling field near the endpoints of the crease shifts a great deal.

Although the optimized fold differs only slightly from its planar counterpart, an important observation can be made—the planar-uniform assumption appears to be violated even in the case when the ratio of fold width to crease length is small, indicating that nonplanar behavior is observed even when bending energy is relatively small.

4.2 Natural Configurations. Now that we have verified that the natural configuration of a circular crease is not a planar-uniform fold, and we turn our attention to solving for a natural configuration.

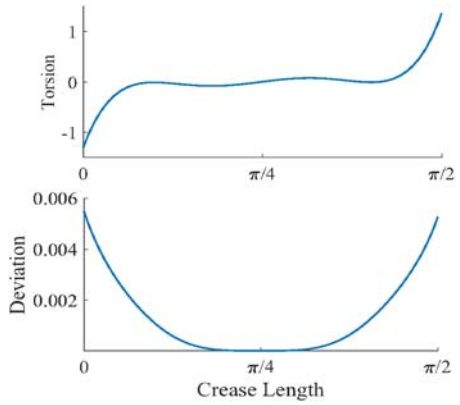

Fig. 8 Optimized torsion function (top) and planar deviation (bottom) for a thin circular crease of width 0.05 units with a fixed fold-angle $\gamma = \pi/2$

We again consider a quarter unit-circle crease, with fold width of 0.8. To find a natural state, we allow both fold-angle and torsion to vary. In accounting for crease energy, we used various values of K (ranging between 1 and 100) and γ_0 (ranging between $\pi/4$ and π). In general, larger values of the stiffness (K) and initial fold-angle (γ_0) result in more folded (larger fold-angle) natural configurations. Figure 9 shows the resulting natural configuration and ruling field for parameter values $K = 50$ and $\gamma_0 = \pi/2$.

The result shows high fidelity to physical models, and one other surprising result is observed: as the values K and γ_0 are varied, the fold angle of the natural form varies but the ruling field remains almost completely fixed. In fact, for parameter values in the previously defined range, the ruling angles β for both left and right fold surfaces show a maximum deviation of 0.02 rad. This deviation could likely be attributed to the truncation error of using a degree-6 Legendre basis to represent torsion and fold angle functions.

This surprising observation hints that even though the natural configuration is neither planar nor uniform, it may remain ruling-rigid foldable throughout its range of motion. This observation appears to agree with physical prototypes, but verifying this conjecture is left to future work.

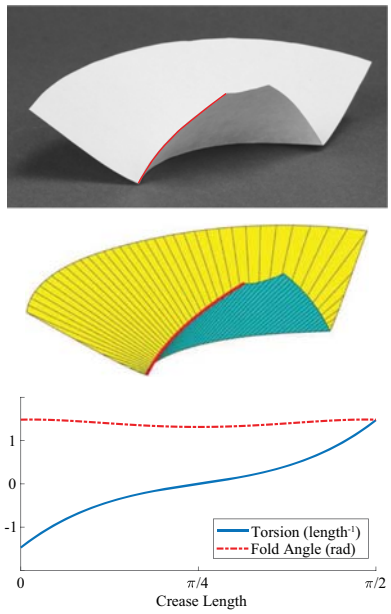

Fig. 9 A physical model (top) and simulated natural configuration using $K = 50$ and $\gamma_0 = \pi/2$ (bottom) for a circular crease of width 0.8 units

We briefly note that the natural configuration of a fold may be altered by varying the width of the fold along the crease. Additionally, methods such as material prestressing [29] may be used to alter the natural configuration and could be used to produce multiple natural fold configurations (i.e., multistable configurations).

4.3 General Curved Folds. The proposed energy method is valid for general curved folds. To illustrate the application of the previously proposed energy method to noncircular creases, Fig. 10 compares a physical model and corresponding simulated natural configuration for a crease defined by curvature $\kappa_g = \cos(s)$ for $s \in [0, 3\pi]$ and of constant width 0.7 units. The simulated natural configuration shows a high degree of fidelity to the physical model.

Additionally, Fig. 11 illustrates the physical and predicted natural configuration of a curved fold with variable width. The crease is defined by curvature $\kappa_g = 4\tan^{-1}(s)$ for $s \in [-1.5, 1.5]$, and the width of fold surface varies linearly between 0.1 and 0.7 units. The simulated natural configuration again shows a high degree fidelity to the physical model, capturing various distinguishing features including the highly nonplanar behavior and decreasing fold angle near the ends.

4.4 Edge of Regression Analysis. We now make observations about the motion of the edge of regression as a fold transitions from a planar-uniform configuration to a natural configuration.

For the planar-uniform circle fold (depicted in Fig. 5), the edge of regression is 1 unit from the crease at each point along the fold, but the inner edge of the fold (near the apex of the cone) is more curved than the outer edge. This is because the value of v_0 is positive for the inner fold surface (since it lies in the direction of the director) and negative for the outer fold surface (since it lies in the opposite direction of the director). Consequently, the inner surface has a higher bending energy than the outer surface. In contrast, functions of v_0 of the natural configuration are negative for both fold surfaces.

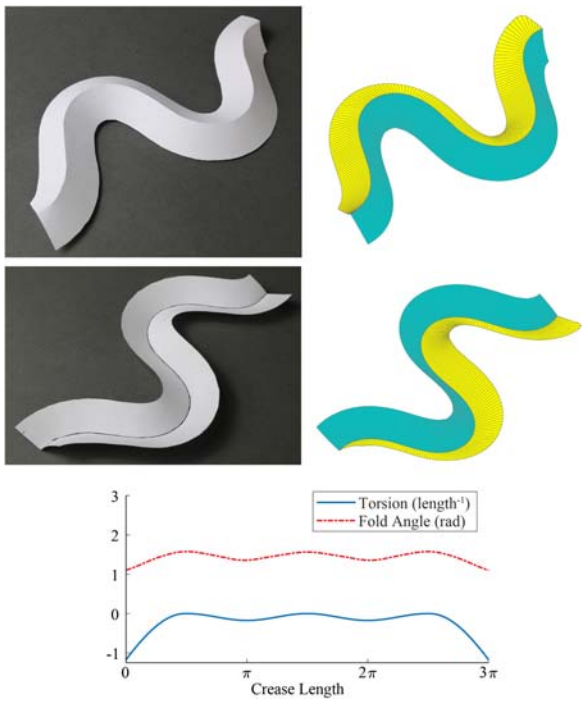

Fig. 10 Physical model (left) and natural simulated configuration using $K = 100$ and $\gamma_0 = \pi/2$ (right) along with the simulated torsion and fold-angle functions (bottom) for a crease with curvature $\kappa_g = \cos(s)$ for $s \in [0, 3\pi]$ of width 0.7 units

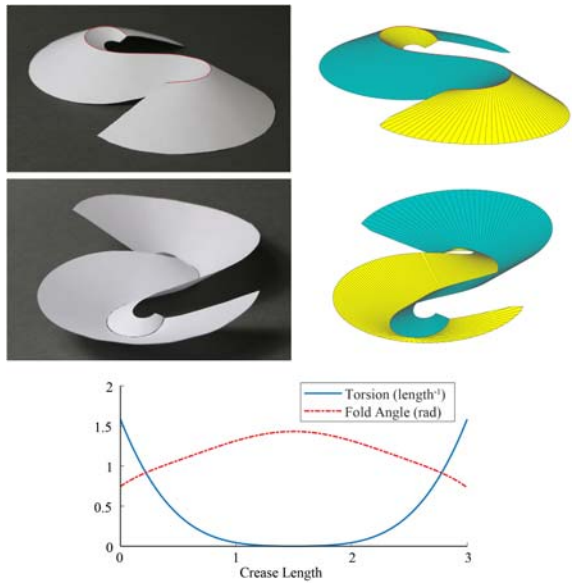

Fig. 11 Physical model (left) and natural simulated configuration using $K = 100$ and $\gamma_0 = \pi/2$ (right) along with the simulated torsion and fold-angle functions (bottom) for a crease with curvature $\kappa_g = 4\tan^{-1}(s)$ for $s \in [-1.5, 1.5]$ and variable fold width

This reduces the bending energy of the inner surface and results in a lower total bending energy.

To further illustrate the relationship between the edge of regression and bending energy, we consider the *ruling energy*, e_R, defined as the bending energy along a ruling line given as follows:

$$e_R = \int \frac{\kappa_p^2(u)}{\Upsilon(u, v)} |\sin\beta(u)|\, \dot{s}\, dv \tag{23}$$

where the bounds of integration are again given by the edge functions. The ruling energy for the quarter circular crease is illustrated in Fig. 12. Notice that by shifting the edge of regression to the side of the crease opposite the fold surface (indicated in the figure by $v_0 < 0$), the ruling energy of the inner surface is reduced significantly.

To understand the conditions that allow a curved fold to assume a configuration where v_0 is negative for both fold surfaces, we consider Eq. (7) under the assumptions that $\kappa_g > 0$ and $\dot{s} = 1$. Thus,

$$v_0 = \frac{\sin\beta}{\kappa_g + \beta'} \tag{24}$$

Assume for a moment that $\beta' = 0$ for both left and right surfaces. Recalling that $\beta_L \in (0, \pi)$ and $\beta_R \in (-\pi, 0)$, we see

$$v_{0,L} = \frac{\sin\beta_L}{\kappa_g} = \frac{\sin|\beta_L|}{\kappa_g}$$

$$v_{0,R} = \frac{\sin\beta_R}{\kappa_g} = -\frac{\sin|\beta_R|}{\kappa_g}$$

Thus, the left surface is *positive biased* while the right surface is *negative biased*. In order to negate $v_{0,L}$, it is therefore required that $\beta_L' < -\kappa_g$. Since β_L is bounded, this is only possible over a finite interval and we can bound the turning angle (θ) of the flat crease

$$\theta = \int \kappa_g < \int \beta_L' < \pi$$

where the turning angle is the total angle the tangent rotates along some length of a curve. Therefore $v_{0,L}$ cannot be negative along the entire crease if the turning angle of the flat crease is greater than π. For folds where θ is greater than π, we have observed that

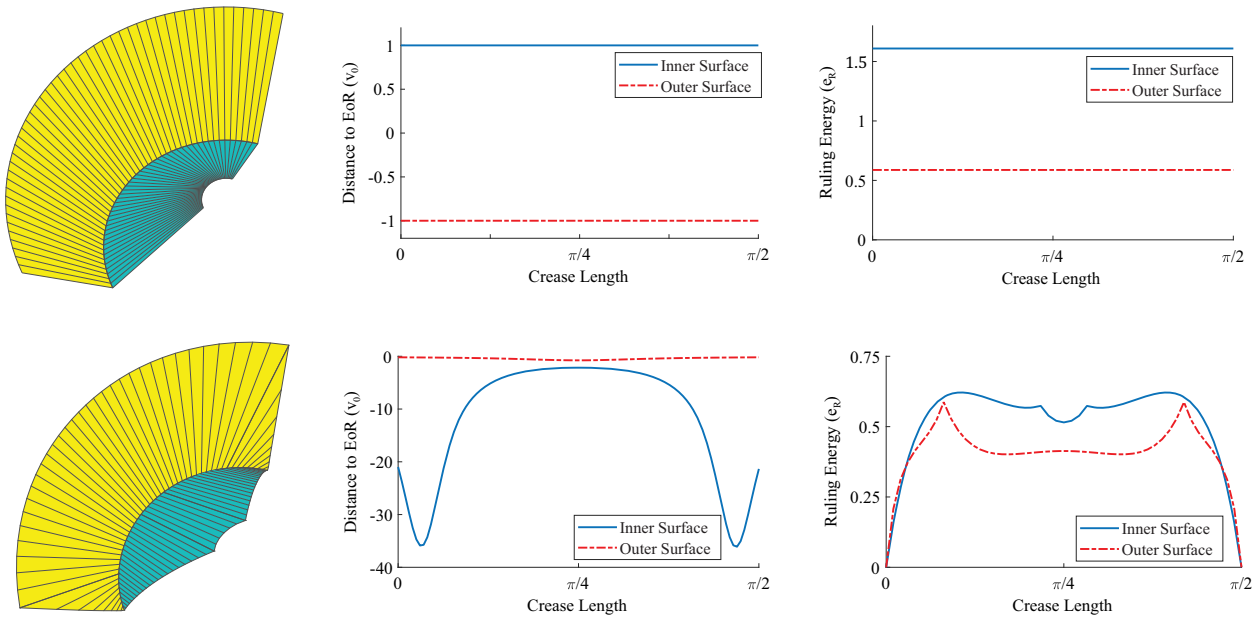

Fig. 12 Planar (top-left) and natural (bottom-left) configurations of a quarter circular crease of width 0.8. The distance to the edge of regression, v_0 (center), and ruling energy (right) are given to illustrate the effect that the location of the edge of regression on the total energy of the fold. Note that the ruling energies are small near the ends of the crease in the natural configurations because the length of the ruling lines decreases toward the ends of the crease.

portions of the fold near the middle of the crease preferentially take planar-uniform configurations while the ends of the crease take nonplanar configurations. These findings are in good agreement with those of Ref. [28] where it was found that as the turning angle is increased, longer sections of planar-uniform behavior are observed near the center of the crease.

We briefly note that whenever $\kappa_g = -\beta'$, v_0 is singular. If v_0 is singular over an interval, the fold surface is locally (on that interval) a generalized cylinder. If v_0 is singular at a point, the ruling line at this point is the boundary between two distinct developable surfaces. This implies that the fold surface consists of multiple developable surfaces joined along ruling lines.

5 Conclusion

We presented novel normalized coordinate equations that simplify curved-fold relationships and facilitate energy analysis of curved folds. These normalized coordinate equations provide a simple and geometrically intuitive framework for understanding curved fold behavior. An energy method was derived based on normalized coordinates to predict natural curved-fold configurations for general curved folds. This energy method revealed that nonplanar behavior lowers surface energy by shifting ruling lines, moving the edge of regression. While other results have recently observed nonplanar behavior in various simple folds [13,27,28], we used normalized coordinates to provide mathematical context and physical intuition for this nonplanar behavior. The method was applied to noncircular and variable width creases and was observed to accurately predict natural fold behavior for general curved folds.

The ability to determine the natural configuration has interesting consequences. For example, identifying the natural configuration of a curved fold allows the orientation of the rulings on the folded surface to be predicted, and the rulings can then be used as hinge lines for developable mechanisms [30]. One of the greatest potential advantages of implementing developable mechanisms on curved-fold surfaces in this way is that it enables 3D structures with complex spatial mechanisms to be manufactured from flat sheets of material. Because a developable mechanism is capable of conforming to a surface, these mechanisms may prove useful for conceal-reveal applications [31] or for integrating structural and functional geometries [32–34].

The normalized coordinate equations and the energy method presented here provide simple and effective tools for predicting natural curved-fold behavior for general curved creases, an ability that will become important as curved-crease origami is used in deployable engineering applications.

Acknowledgment

This paper is based on work supported by the National Science Foundation (NSF) and the Air Force Office of Scientific Research through NSF Grant No. EFRI-ODISSEI-1240417, NSF Grant No. 1663345, and the NSF Graduate Research Fellowship Program under Grant No. 1247046. R. J. L. acknowledges support from the NSF and Air Force Office of Scientific Research through grants EFRI-ODISSEI-1240417, EFRI-ODISSEI-1240441, EFRI-ODISSEI-1332249, and EFRI-ODISSEI-1332271.

References

[1] Demaine, E. D., and O'Rourke, J., 2008, *Geometric Folding Algorithms: Linkages, Origami, Polyhedra*, Cambridge University Press, Cambridge.
[2] Zhao, Y., Kanamori, Y., and Mitani, J., 2018, "Design and Motion Analysis of Axisymmetric 3d Origami With Generic Six-Crease Bases," Comput. Aided Geom. Des., **59**, pp. 86–97.
[3] Hanna, B. H., Magleby, S. P., Lang, R. J., and Howell, L. L., 2015, "Force–Deflection Modeling for Generalized Origami Waterbomb-Base Mechanisms," ASME J. Appl. Mech., **82**(8), p. 081001.
[4] Lee, T.-U., and Gattas, J. M., 2016, "Geometric Design and Construction of Structurally Stabilized Accordion Shelters," ASME J. Mech. Rob., **8**(3), p. 031009.
[5] Feng, H., Ma, J., Chen, Y., and You, Z., 2018, "Twist of Tubular Mechanical Metamaterials Based on Waterbomb Origami," Sci. Rep., **8**(1), p. 9522.
[6] Chen, Y., Peng, R., and You, Z., 2015, "Origami of Thick Panels," Science, **349**(6246), pp. 396–400.
[7] Chen, Z., Wu, T., Nian, G., Shan, Y., Liang, X., Jiang, H., and Qu, S., 2019, "Ron Resch Origami Pattern Inspired Energy Absorption Structures," ASME J. Appl. Mech., **86**(1), p. 011005.
[8] Ma, J., and You, Z., 2014, "Energy Absorption of Thin-Walled Square Tubes With a Prefolded Origami Pattern Part I: Geometry and Numerical Simulation," ASME J. Appl. Mech., **81**(1), p. 011003.
[9] Zhou, C., Jiang, L., Tian, K., Bi, X., and Wang, B., 2017, "Origami Crash Boxes Subjected to Dynamic Oblique Loading," ASME J. Appl. Mech., **84**(9), p. 091006.
[10] Zhou, C., Ming, S., Li, T., Wang, B., and Ren, M., 2018, "The Energy Absorption Behavior of Cruciforms Designed by Kirigami Approach," ASME J. Appl. Mech., **85**(12), p. 121008.

[11] Tang, C., Bo, P., Wallner, J., and Pottmann, H., 2016, "Interactive Design of Developable Surfaces," ACM Trans. Graph., **35**(2), p. 12.
[12] Kilian, M., Flöry, S., Chen, Z., Mitra, N. J., Sheffer, A., and Pottmann, H., 2008, "Curved Folding," ACM Trans. Graph., **27**(3), p. 75.
[13] Lee, T.-U., You, Z., and Gattas, J. M., 2018, "Elastica Surface Generation of Curved-Crease Origami," Int. J. Solids Struct. **136-137**, pp. 13–27.
[14] Fuchs, D., and Tabachnikov, S., 1999, "More on Paperfolding," Am. Math. Mon., **106**(1), pp. 27–35.
[15] Duncan, J. P., and Duncan, J., 1982, "Folded Developables," Proc. R. Soc. Lond. Math. Phys. Sci., **383**(1784), pp. 191–205.
[16] Struik, D. J., 1961, *Lectures on Classical Differential Geometry*, Courier Dover Publications, New York.
[17] Lang, R., Nelson, T., Magleby, S., and Howell, L., 2017, "Kinematics and Discretization of Curved Fold Mechanisms," ASME 2017 IDETC/CIE, No. IDETC2017-59747, ASME.
[18] Aumann, G., 2003, "A Simple Algorithm for Designing Developable Bzier Surfaces," Comput. Aided Geom. Des., **20**(8), pp. 601–619 (in memory of Professor J. Hoschek).
[19] Weisstein, E. W., 2002, *CRC Concise Encyclopedia of Mathematics*, CRC Press, Boca Raton, FL.
[20] Mitani, J., and Igarashi, T., 2011, "Interactive Design of Planar Curved Folding by Reflection," Proceedings of PG 2011, Kaohsiung, Taiwan, Sept. 21–23.
[21] Demaine, E. D., Demaine, M. L., Huffman, D. A., Koschitz, D., and Tachi, T., 2014, "Designing Curved-Crease Tessellations of Lenses: Qualitative Properties of Rulings," 6th International Meeting on Origami in Science, Mathematics and Education (OSME 2014), Tokyo, Aug., pp. 10–13.
[22] Dias, M. A., 2012, "Swelling and Folding as Mechanisms of 3d Shape Formation in Thin Elastic Sheets," PhD thesis, University of Massachusetts Amherst, Amherst, MA.
[23] Nelson, T. G., Lang, R. J., Pehrson, N. A., Magleby, S. P., and Howell, L. L., 2016, "Facilitating Deployable Mechanisms and Structures Via Developable Lamina Emergent Arrays," ASME J. Mech. Rob., **8**(3), p. 031006.
[24] Abbena, E., Salamon, S., and Gray, A., 2006, *Modern Differential Geometry of Curves and Surfaces With Mathematica*, CRC Press, Boca Raton, FL.
[25] Verbeek, P. W., and Van Vliet, L. J., 1993, "Curvature and Bending Energy in Digitized 2D and 3D Images," 8th Scandinavian Conference on Image Analysis, Tromso, Norway, May 25, pp. 1403–1410.
[26] Wang, W., and Qui, X., 2017, "Coupling of Creases and Shells," ASME J. Appl. Mech., **85**(1), p. 011009.
[27] Lee, T. U., You, Z., and Gattas, J. M., 2018, "Curved-Crease Origami With Multiple States," Origami 7: Seventh International Meeting of Origami Science, Mathematics, and Education, Oxford, Sept. 5–7.
[28] Woodruff, S. R., and Filipov, E. T., 2018, "Structural Analysis of Curved Folded Deployables," ASCE Earth and Space Conference, Cleveland, OH, Apr. 9–12, p. 793.
[29] Seffen, K. A., and Guest, S. D., 2011, "Prestressed Morphing Bistable and Neutrally Stable Shells," ASME J. Appl. Mech., **78**(1), p. 011002.
[30] Nelson, T. G., Zimmerman, T. K., Magleby, S. P., Lang, R. J., and Howell, L. L., 2019, "Developable Mechanisms on Developable Surfaces," Sci. Rob., **4**(27), p. 5171.
[31] DeFigueiredo, B., Pehrson, N. A., Tolman, K., Crampton, E., Magleby, S. P., and Howell, L. L., 2019, "Origami-Based Design of Conceal-and-Reveal Systems," ASME J. Mech. Rob., **11**(2), p. 020904.
[32] Cai, J., Qian, Z., Jiang, C., Feng, J., and Xu, Y., 2016, "Mobility and Kinematic Analysis of Foldable Plate Structures Based on Rigid Origami," ASME J. Mech. Rob., **8**(6), p. 064502.
[33] Cai, J., Zhang, Q., Feng, J., and Xu, Y., 2018, "Modeling and Kinematic Path Selection of Retractable Kirigami Roof Structures," Comput. Aided Civil Infrastruct. Eng., **34**(4), pp. 352–363.
[34] Jianguo, C., Yangqing, L., Ruijun, M., Jian, F., and Ya, Z., 2017, "Nonrigidly Foldability Analysis of Kresling Cylindrical Origami," ASME J. Mech. Rob., **9**(4), p. 041018.